Is the Orbital-Selective Mott Phase Stable against Interorbital Hopping?

Fabian B. Kugler and Gabriel Kotliar

Is the orbital-selective Mott phase stable against interorbital hopping?

Fabian B. Kugler[1] and Gabriel Kotliar[1, 2]

[1]*Department of Physics and Astronomy, Rutgers University, Piscataway, NJ 08854, USA*
[2]*Condensed Matter Physics and Materials Science Department, Brookhaven National Laboratory, Upton, NY 11973, USA*
(Dated: June 10, 2022)

The localization–delocalization transition is at the heart of strong correlation physics. Recently, there is great interest in multiorbital systems where this transition can be restricted to certain orbitals, leading to an orbital-selective Mott phase (OSMP). Theoretically, the OSMP is widely studied for kinetically decoupled orbitals, but the effect of interorbital hopping remains unclear. Here, we show how nonlocal interorbital hopping leads to local hybridization in single-site dynamical mean-field theory (DMFT). Under fairly general circumstances, this implies that, at zero temperature, the OSMP, involving the Mott-insulating state of one orbital, is unstable against interorbital hopping to another, metallic orbital. We further show that the coherence scale below which all electrons are itinerant is very small and gets exponentially suppressed even if the interorbital hopping is not overly small. Within this framework, the OSMP with interorbital hopping may thus reach down to extremely low temperatures T but not to $T = 0$. Accordingly, it is part of a coherence–incoherence crossover and not a quantum critical point. We present analytical arguments supported by numerical results using the numerical renormalization group as DMFT impurity solver. We also compare our findings with previous slave-spin studies.

The evolution of the electronic structure from localized to itinerant is a fundamental problem in condensed-matter physics and relevant to many interesting materials. It continues to receive much experimental attention as the transition region between localized and delocalized behavior hosts remarkable phenomena, like high-temperature superconductivity [1–3].

Recently, there is focus on multiorbital systems, triggered by the observation of orbital selectivity whereby a subset of orbitals (denoted "heavy") has much larger effective mass than another group (denoted "light"). An illustrative example under current study is $FeTe_{1-x}Se_x$ [4–7]. There, among the t_{2g} orbitals, the d_{xy} is the heaviest. A central idea in this field is the orbital-selective Mott phase (OSMP) [8] where heavy electrons are Mott-localized and coexist with itinerant light electrons. This idea is relevant to numerous model systems and materials [9–19]. Often, a small difference among the orbitals at the one-particle level is drastically amplified by many-body correlations. Importantly, a sharp localization–delocalization boundary can only be defined at zero temperature, $T=0$, via the participation of charge carriers in the volume of the Fermi surface.

The OSMP has been investigated intensively using dynamical mean-field theory (DMFT) [20, 21] and slave-spin methods [22–24]. There is consensus that the OSMP is realized within these methods in the absence of hopping matrix elements between different orbitals [25–30]. This assumption is natural for local matrix elements (which are zero in high-symmetry situations [31]) but not for nonlocal ones (which are allowed by symmetry) [35]. In realistic materials estimations, the interorbital nonlocal hopping amplitudes are often comparable to those of the light electrons [36].

Earlier attempts to study the OSMP including interorbital hopping t_{io} resulted in different pictures. Using slave spins, Refs. [34, 39] concluded that the OSMP survives finite t_{io} at $T = 0$, while LDA+DMFT calculations of FeTe using a Monte Carlo impurity solver [40] [41] argued for a smooth crossover, where localization occurs only at sufficiently high
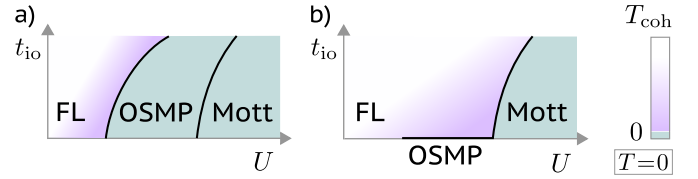

FIG. 1. Two possible scenarios, a) and b), for the zero-temperature ($T = 0$) phase diagram of multiorbital systems as a function of Coulomb repulsion U and interorbital hopping t_{io}. Here, we provide evidence for scenario b) in which any finite t_{io} replaces the OSMP by a Fermi liquid (FL). The coherence scale T_{coh}, below which all electrons are itinerant, is very low close to the OSMP and Mott phase.

T [44]. These two pictures are sketched in Fig. 1 as qualitative $T=0$ phase diagrams. They also lead to different behavior at finite temperature: In the first case, one expects definite scaling behavior tied to a coherence scale T_{coh} which vanishes when a control parameter x (e.g., interaction strength or doping) reaches a critical value x_c. But the second scenario predicts a coherence–incoherence crossover where there is no such x_c and T_{coh} stays finite.

Here, we settle this issue within the paramagnetic single-site DMFT in favor of the second scenario. We provide analytic arguments why any finite t_{io} destabilizes the OSMP, based on the DMFT equations. The underlying mechanism has a simple physical interpretation, and we show that the same mechanism is obstructed within the more approximate slave-spin methods (thus explaining the results of Refs. [34, 39]). We obtain an exact numerical solution of the DMFT equations for a multiorbital model with interorbital hopping using the numerical renormalization group (NRG) [47]. This method is necessary to reach arbitrarily low T and to show that T_{coh}, while always finite, can be extremely small.

The basic argument is: the DMFT views correlated systems as a collection of atoms, each of which hybridizes with the environment given by the rest of the lattice. The low-energy hybridization plays a key role: it is generically finite for Fermi liquids and vanishes for Mott insulators. We will show that the

low-energy hybridization of an electron in any orbital is finite as long as it can hop to another, delocalized orbital and back. This process is described by the momentum-dependent interorbital hopping $\epsilon_{\boldsymbol{k}}^{\mathrm{io}}$ and the momentum- and frequency-dependent density of states $\mathcal{A}_{\boldsymbol{k}\nu}^{\mathrm{lt}}$ of a light orbital, as $\sum_{\boldsymbol{k}}(\epsilon_{\boldsymbol{k}}^{\mathrm{io}})^2\mathcal{A}_{\boldsymbol{k}\nu}^{\mathrm{lt}}$. It is this low-energy hybridization which destabilizes the Mott state in favor of a Fermi-liquid ground state. Below, we derive the hybridization formula for a two-orbital model, discuss the coherence scale, and illustrate the consequences with numerical results.

Model—We consider a multiorbital Hubbard Hamiltonian

$$\hat{H} = \sum_{ijnm\sigma} \hat{d}_{in\sigma}^{\dagger} h_{ij}^{nm} \hat{d}_{jm\sigma} + \sum_{i} \hat{H}_{\mathrm{int}}[\hat{d}_{in\sigma}], \quad (1)$$

where $\hat{d}_{in\sigma}^{\dagger}$ creates an electron at site i, in orbital n, and with spin σ. The hopping matrix h_{ij}^{nm} features nonlocal ($i \neq j$) interorbital ($n \neq m$) hopping; its Fourier transform is $h_{\boldsymbol{k}}^{nm}$. $\hat{H}_{\mathrm{int}}$ denotes the local interaction. In single-site DMFT, correlations are assumed to be local [20]. The propagator reads $\boldsymbol{G}_{\boldsymbol{k}\nu} = [\nu+\mu-\boldsymbol{h}_{\boldsymbol{k}}-\boldsymbol{\Sigma}_{\nu}]^{-1}$ with the chemical potential μ and the retarded, matrix-valued self-energy $\boldsymbol{\Sigma}_{\nu}$. In sufficiently symmetric situations, the orbitals can be chosen orthogonal, such that local one-particle objects are diagonal in orbital space [21, 48]. This includes $\boldsymbol{G}_{\mathrm{loc},\nu} = \sum_{\boldsymbol{k}} \boldsymbol{G}_{\boldsymbol{k}\nu}$, $\boldsymbol{\Sigma}_{\nu}$, and the on-site energies $\boldsymbol{\epsilon}_d = \sum_{\boldsymbol{k}} \boldsymbol{h}_{\boldsymbol{k}} - \mu$. Momentum sums are normalized: $\sum_{\boldsymbol{k}} 1 = 1$.

A minimal model for the OSMP has two (orthogonal) orbitals, a light (lt) and a heavy (hv) orbital. We write the general hopping matrix, including the interorbital hopping $\epsilon_{\boldsymbol{k}}^{\mathrm{io}}$, as

$$\boldsymbol{h}_{\boldsymbol{k}} - \mu = \begin{pmatrix} \epsilon_{\boldsymbol{k}}^{\mathrm{lt}} & \epsilon_{\boldsymbol{k}}^{\mathrm{io}} \\ \epsilon_{\boldsymbol{k}}^{\mathrm{io}} & \epsilon_{\boldsymbol{k}}^{\mathrm{hv}} \end{pmatrix}, \quad (2)$$

The local propagator follows from a 2×2 matrix inversion as

$$\boldsymbol{G}_{\mathrm{loc},\nu} = \sum_{\boldsymbol{k}} \frac{1}{\prod_{n=\mathrm{lt,hv}}[\nu - \epsilon_{\boldsymbol{k}}^n - \Sigma_{\nu}^n] - (\epsilon_{\boldsymbol{k}}^{\mathrm{io}})^2}$$
$$\times \begin{pmatrix} \nu - \epsilon_{\boldsymbol{k}}^{\mathrm{hv}} - \Sigma_{\nu}^{\mathrm{hv}} & -\epsilon_{\boldsymbol{k}}^{\mathrm{io}} \\ -\epsilon_{\boldsymbol{k}}^{\mathrm{io}} & \nu - \epsilon_{\boldsymbol{k}}^{\mathrm{lt}} - \Sigma_{\nu}^{\mathrm{lt}} \end{pmatrix}. \quad (3)$$

For our numeric results, we use the simplistic expressions

$$\epsilon_{\boldsymbol{k}}^n = -2t_n[\cos(k_x) + \cos(k_y) + \cos(k_z)] - \mu,$$
$$\epsilon_{\boldsymbol{k}}^{\mathrm{io}} = -2t_{\mathrm{io}}[\cos(k_x) - \cos(k_y)], \quad (4)$$

for which diagonality of $\boldsymbol{\epsilon}_d$ and $\boldsymbol{G}_{\mathrm{loc},\nu}$ is obvious. However, our general arguments are independent of the choice of Eq. (4).

DMFT equations—In DMFT, the lattice model is mapped onto an impurity model. We call the (orbital-diagonal) impurity propagator $\boldsymbol{g}_{\nu} = [\nu - \boldsymbol{\epsilon}_d - \boldsymbol{\Delta}_{\nu} - \boldsymbol{\Sigma}_{\nu}]^{-1}$, where $\boldsymbol{\Delta}_{\nu}$ is the retarded hybridization function. The appropriate $\boldsymbol{\Delta}_{\nu}$ is found by iteration until self-consistency between the local lattice propagator and its impurity counterpart, $\boldsymbol{G}_{\mathrm{loc},\nu} = \boldsymbol{g}_{\nu}$, is reached.

The diagonal elements of the local propagator are ($m \neq n$)

$$G_{\mathrm{loc},\nu}^n = \sum_{\boldsymbol{k}} \frac{1}{r_{\boldsymbol{k}\nu}^n - \Sigma_{\nu}^n}, \quad r_{\boldsymbol{k}\nu}^n = \nu - \epsilon_{\boldsymbol{k}}^n - \frac{(\epsilon_{\boldsymbol{k}}^{\mathrm{io}})^2}{\nu - \epsilon_{\boldsymbol{k}}^m - \Sigma_{\nu}^m}, \quad (5)$$
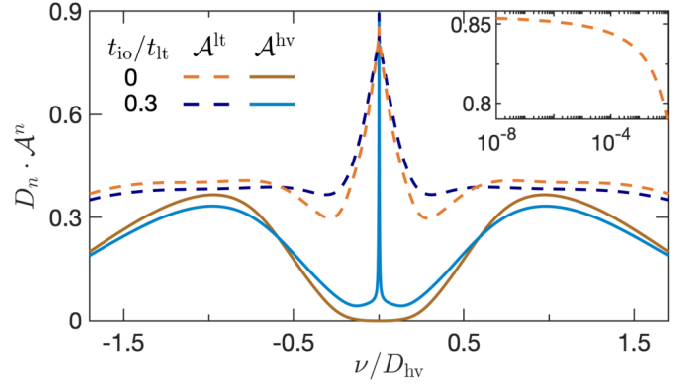

FIG. 2. Spectral functions $\mathcal{A}^n$ for the light and heavy orbital. At $t_{\mathrm{io}} = 0$, we find an OSMP with $\mathcal{A}^{\mathrm{hv}}$ gapped. Finite t_{io} destabilizes the OSMP as $\mathcal{A}^{\mathrm{hv}}$ develops a thin quasiparticle peak. Inset: In the OSMP, $\lim_{\nu\to 0} \mathcal{A}_{\nu}^{\mathrm{lt}}$ converges only asymptotically [30, 49].

taken from Eq. (3). The hybridization in the bare impurity propagator is then determined according to $G_{\mathrm{loc},\nu}^n = g_{\nu}^n$. With $1/g_{0,\nu}^n = \nu - \epsilon_d^n - \Delta_{\nu}^n$, Δ_{ν}^n can be found from

$$\frac{1}{g_{0,\nu}^n} = \Sigma_{\nu}^n + \frac{1}{G_{\mathrm{loc},\nu}^n} = \frac{\sum_{\boldsymbol{k}} \frac{r_{\boldsymbol{k}\nu}^n}{r_{\boldsymbol{k}\nu}^n - \Sigma_{\nu}^n}}{\sum_{\boldsymbol{k}} \frac{1}{r_{\boldsymbol{k}\nu}^n - \Sigma_{\nu}^n}}. \quad (6)$$

This intermediate result is key for the following discussion. It gives the hybridization components for a general two-orbital system [Eq. (2)] according to the DMFT self-consistency condition. We reshuffled the self-energy from the numerator into the denominator, but no approximation was made thus far.

While Eq. (6) holds at self-consistency, during the DMFT iteration, it is used to update Δ_{ν}^n from a given solution of the impurity model (yielding Σ_{ν}^n) to the next. We can briefly check the noninteracting case, $\Sigma_{\nu}^n = 0$, for which DMFT self-consistency is trivial. There, Eq. (6) correctly yields $g_{0,\nu}^n = \sum_{\boldsymbol{k}} \frac{1}{r_{\boldsymbol{k}\nu}^n}$. Next, we use Eq. (6) to investigate whether the OSMP is stable against interorbital hopping. To this end, we start from a converged DMFT solution with $t_{\mathrm{io}} = 0$ realizing the OSMP. Then, we turn on t_{io} to check if the Mott insulator persists.

Indeed, starting at $t_{\mathrm{io}} = 0$ and setting, e.g., $t_{\mathrm{hv}} \ll t_{\mathrm{lt}}$ at large interaction and half filling, the heavy orbital is Mott-insulating while the light orbital remains metallic. The Mott insulator is signaled by a gap in the local density of states $\mathcal{A}_{\nu}^{\mathrm{hv}}$, where $-\pi\mathcal{A}_{\nu}^n = \mathrm{Im}\, G_{\mathrm{loc},\nu}^n = \mathrm{Im}\, g_{\nu}^n$, and a divergent effective mass, i.e., $\lim_{\nu\to 0} |\Sigma_{\nu}^{\mathrm{hv}}| = \infty$. The impurity solution yielding $\boldsymbol{g}_{\nu}$ and $\boldsymbol{\Sigma}_{\nu}$ is determined by the hybridization $\boldsymbol{\Delta}_{\nu}$ with spectral weights $\mathcal{A}_{\Delta,\nu}^n = -\mathrm{Im}\,\Delta_{\nu}^n/\pi$. In most cases [11, 50–53], a Fermi-liquid ground state is found if all $\mathcal{A}_{\Delta,\nu}^n$ are finite around $\nu = 0$, while a Mott-insulating orbital requires a gapped $\mathcal{A}_{\Delta,\nu}^n$.

Now, we perform the first DMFT update, starting from the OSMP solution but setting $t_{\mathrm{io}} \neq 0$. It is clear from Eq. (5) that $\lim_{\nu\to 0} |\Sigma_{\nu}^{\mathrm{hv}}| = \infty$ makes $G_{\mathrm{loc},\nu=0}^n$ for both n independent of $\epsilon_{\boldsymbol{k}}^{\mathrm{io}}$, so that, in particular, $\mathcal{A}_{\nu}^{\mathrm{hv}}$ remains gapped. However, the result of the next iteration is determined by $\mathcal{A}_{\Delta}^n$, not $\mathcal{A}^n$. The divergent self-energy also simplifies the updated hybridization

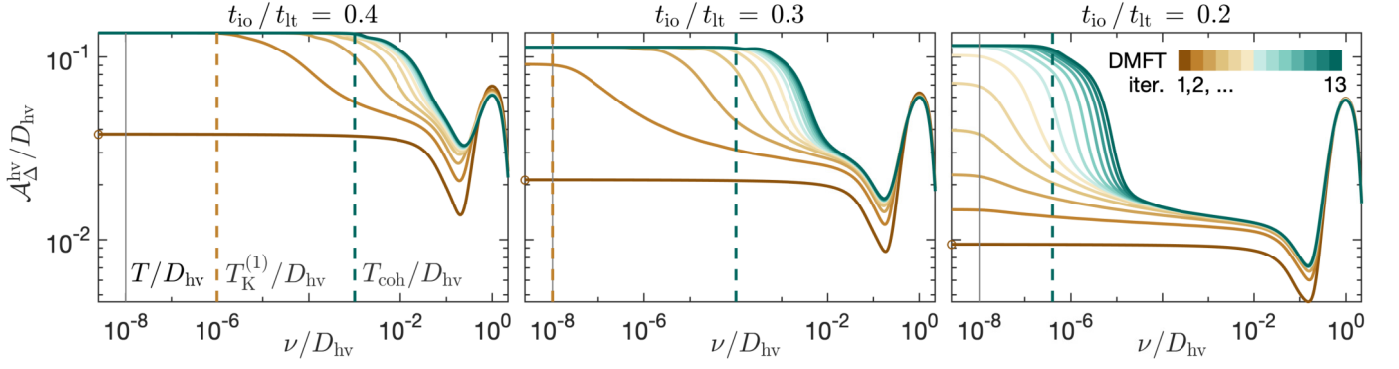FIG. 3. Hybridization function $\mathcal{A}_\Delta$ in the heavy orbital for several DMFT iterations with finite t_{io}, starting from the OSMP solution at $t_{io}=0$. Circles on the vertical axis give values $(t_{io}/t_{lt})^2 \times$ const according to Eq. (7). Dashed vertical lines indicate the coherence scale after the first DMFT iteration, $T_K^{(1)}$, and after the last DMFT iteration, T_{coh}. For $t_{io}/t_{lt}=0.2$, $T_K^{(1)} \ll T$ and $T_{coh} \gtrsim T$; this opens a window of intermediate energies $|\nu| > T_{coh}$ with OSMP-like features (cf. Fig. 4).

function. In the limit $\nu \to 0$ within the OSMP, Eq. (6) yields

$$|\Sigma_\nu^{hv}| \to \infty: \quad \frac{1}{g_{0,\nu}^{hv}} = \sum_{\boldsymbol{k}} r_{\boldsymbol{k}\nu}^{hv}, \quad \Delta_\nu^{hv} = \sum_{\boldsymbol{k}} (\epsilon_{\boldsymbol{k}}^{io})^2 G_{\boldsymbol{k}\nu}^{lt}. \quad (7)$$

For the second relation, $\nu - \epsilon_d^{hv}$ in $1/g_{0,\nu}^{hv}$ and $\sum_{\boldsymbol{k}}(\nu - \epsilon_{\boldsymbol{k}}^{hv})$ from $r_{\boldsymbol{k}}^{hv}$ cancel, and $G_{\boldsymbol{k}\nu}^{lt} = 1/(\nu - \epsilon_{\boldsymbol{k}}^{lt} - \Sigma_\nu^{lt})$ when Σ_ν^{hv} diverges. Equation (7) is our main result. Assuming a divergent Σ_ν^{hv} at low frequencies, Δ_ν^{hv} retains a finite value, independent of Σ_ν^{hv}. Since a finite hybridization yields a Fermi-liquid ground state in fairly general impurity models [11, 50–53], we find that, with $\mathcal{A}_{\Delta,\nu}^{hv} = \sum_{\boldsymbol{k}}(\epsilon_{\boldsymbol{k}}^{io})^2 \mathcal{A}_{\boldsymbol{k}\nu}^{lt} > 0$, the Mott-insulating state of the heavy orbital is unstable against interorbital hopping. In further DMFT iterations, a quasiparticle peak in the heavy orbital will form, and Σ_ν^{hv} will no longer diverge. In the Supplemental Material [54], we show that Eq. (7) holds analogously for any number of orbitals, and we provide a free-energy functional to illustrate the universal nature of the effect described above.

We next include a temperature/energy coherence scale below which the Fermi-liquid properties are found. In the single-impurity Anderson model with large interaction U and (non-singular) hybridization $\mathcal{A}_\Delta$, this scale is the Kondo temperature $T_K \propto \exp(-\alpha U/\mathcal{A}_{\Delta,\nu=0})$ [55]. Similar behavior is expected for our model, albeit it with an effective $\tilde{U}$ encoding further microscopic parameters (like Hund's coupling J) [56]. For the first DMFT iteration after switching from $t_{io}=0$ to $t_{io} \neq 0$, we have $\mathcal{A}_{\Delta,\nu=0}^{hv} \propto t_{io}^2/t_{lt}$ from Eq. (7) and thus $T_K^{(1)} \propto \exp[-\alpha\tilde{U}t_{lt}/t_{io}^2] = c^{(t_{lt}/t_{io})^2}$, with $c \propto \exp[-\alpha\tilde{U}/t_{lt}]$ reminiscent of a single-orbital Kondo scale. This shows that the coherence scale for the first DMFT iteration after the OSMP can be extremely small. In the next iterations, Σ_ν^{hv} no longer diverges, and $\mathcal{A}_{\Delta,\nu=0}^{hv}$ cannot be deduced as easily. However, it is clear that delocalization of the heavy orbital will open more hybridization channels, so that $T_K^{(1)}$ becomes a lower bound for the actual coherence scale after DMFT convergence, $T_{coh} \geq T_K^{(1)}$.

Numerical results—We now turn to numerical results for the model of Eqs. (1), (2) and (4). We denote the half-bandwidth of $\epsilon_{\boldsymbol{k}}^n$ by $D_n = 6t_n$ and consider two half-filled orbitals with $D_{lt}/D_{hv}=2$. $D_{hv}=1$ is our energy unit, $T=10^{-8}$, and $\hat{H}_{int}$

is given by the Kanamori Hamiltonian [54] with parameters $U=2.4$ and $J=0.4$ [11]. We use NRG as a real-frequency impurity solver for DMFT [54] and assume paramagnetism.

To set the stage, Fig. 2 shows two sets of spectral functions $\mathcal{A}^n$ for different interorbital hopping. Our interaction parameters are such that $t_{io}=0$ realizes an OSMP, where $\mathcal{A}^{hv}$ has a gap while $\mathcal{A}^{lt}$ has a peak at $\nu=0$. Coupled to unscreened magnetic moments, the metallic orbital at $T=0$ behaves as a singular Fermi liquid [30, 49], where $\lim_{\nu\to0} \mathcal{A}_\nu^{lt}$ converges only asymptotically (see inset) and formally $Z_{lt}=0$. For finite t_{io}, $\mathcal{A}^{hv}$ develops a narrow quasiparticle peak, replacing the OSMP by a Fermi-liquid ground state. Nevertheless, at larger energies $|\nu| \gtrsim 10^{-2}$, the two sets of spectral functions for $t_{io}=0$ and $t_{io} \neq 0$ are very similar. Particularly, pronounced Hubbard bands in $\mathcal{A}^{hv}$ exist in both phases [58].

Figure 3 illustrates our instability argument. It shows $\mathcal{A}_\Delta^{hv}$ for several DMFT iterations with finite t_{io} starting from the OSMP solution at $t_{io}=0$. In the first iteration, $\mathcal{A}_{\Delta,\nu}^{hv} \propto (t_{io}/t_{lt})^2$ according to Eq. (7). The resulting metallic state leads to an increased hybridization for the next iteration. Its coherence scale (below which, e.g., $\mathcal{A}_\nu^n$ converge) roughly follows $T_K^{(1)} \propto c^{(t_{lt}/t_{io})^2}$. For $t_{io}/t_{lt}=0.2$, $T_K^{(1)} \ll T$, so that $\mathcal{A}_{\Delta,\nu}^{hv}$ for the next iteration converges below T only. In the subsequent DMFT iterations, the hybridization further builds up until the actual coherence scale $T_{coh} \geq T_K^{(1)}$ is established. For $t_{io}/t_{lt}=0.2$, $T_{coh} \gtrsim T$ is very low, and OSMP-like behavior persists for $|\nu| > T_{coh}$.

Indeed, Fig. 4 shows the spectral functions and self-energies after DMFT convergence. For all $t_{io}>0$, a Fermi-liquid ground state is obtained, with a finite quasiparticle peak obeying Luttinger pinning [60] $\mathcal{A}_{\nu=0}^n = \rho_{\nu=0}^n$ and self-energies having a linear real part. At the lowest $t_{io}>0$, however, both properties are fulfilled only at very low energies $|\nu| < T_{coh} \sim 4 \cdot 10^{-7}$ (even though $\mathcal{A}^{lt}$ increases most strongly around $|\nu| \sim 10^{-1}$). For $|\nu| > T_{coh}$, the system is hardly distinguishable from the OSMP: in an intermediate regime of around four orders of magnitude, $\mathcal{A}_\nu^{hv}$ almost vanishes and Σ_ν^{lt} follows the logarithmic behavior of the OSMP [30, 49]. While the quasiparticle weights $Z_n = 1/(1 - \partial_\nu \mathrm{Re}\,\Sigma_\nu^n|_{\nu=0})$ are already on the percent
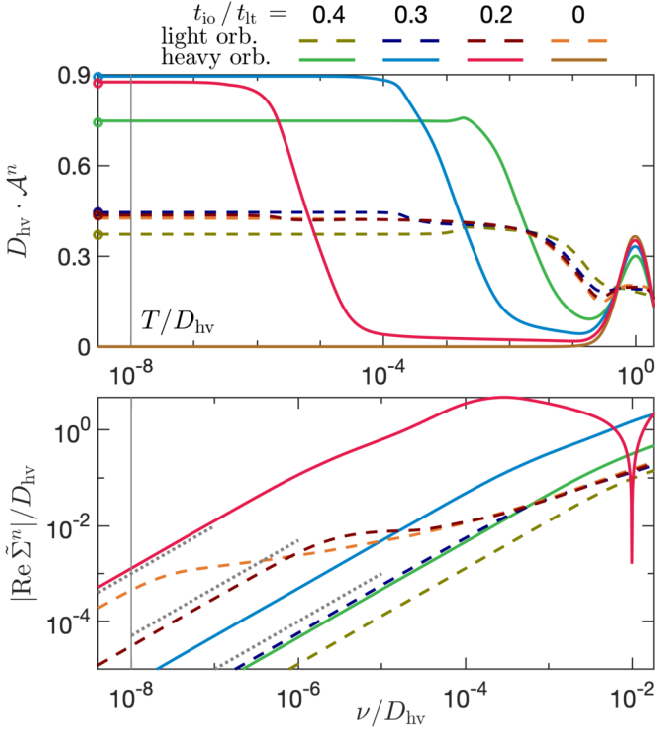
FIG. 4. Spectral functions $\mathcal{A}_\nu$ and self-energies $\tilde\Sigma_\nu = \Sigma_\nu - \Sigma_{\nu=0}$ after DMFT convergence. For $t_{\mathrm{io}}/t_{\mathrm{lt}} \in \{0.4, 0.3, 0.2\}$, Fermi-liquid behavior with $\mathcal{A}_{\nu=0}$ obeying Luttinger pinning (circles) and linear Re $\tilde\Sigma$ is seen below coherence scales of roughly 10^{-3}, 10^{-4}, and $4 \cdot 10^{-7}$, respectively (cf. Fig. 3). For $t_{\mathrm{io}}/t_{\mathrm{lt}} = 0.2$ and $10^{-5} < \nu/D_{\mathrm{hv}} < 10^{-1}$, $\mathcal{A}^{\mathrm{hv}}$ almost vanishes and Re $\tilde\Sigma^{\mathrm{lt}}$ perfectly follows the logarithmic behavior [30, 49] of the $t_{\mathrm{io}} = 0$ OSMP. The three dotted lines indicate $\kappa\nu$, with $\kappa = 10^2, 5 \cdot 10^3, 10^5$ from bottom to top.

level for $t_{\mathrm{io}}/t_{\mathrm{lt}} = 0.3$, they reach values as low as 10^{-3} for the light and 10^{-5} for the heavy orbital at $t_{\mathrm{io}}/t_{\mathrm{lt}} = 0.2$. Decreasing t_{io} further, an OSMP is recovered as $T_{\mathrm{coh}} < T = 10^{-8}$.

Comparison with slave spins—We finally compare our results to previous slave-spin studies which found the OSMP to be stable against interorbital hopping [39]. Slave-spin approaches decompose the physical fermions $\hat{d}$ into a bosonic slave-spin operator $\hat{b}$ and a slave fermion $\hat{f}^\dagger$, $\hat{d}^\dagger_{im\sigma} = \hat{b}_{im\sigma}\hat{f}^\dagger_{im\sigma}$. It was shown that minimizing the mean-field decoupled free energy in slave-spin approaches is equivalent to a DMFT-like treatment where the slave-spin impurity solver yields the quasiparticle weight and DMFT self-consistency is imposed on the slave fermions [34] [see their Eq. (30)].

Expressions for the f fermions follow from those of the d fermions by expanding the self-energy to linear order, $\Sigma^n_\nu \approx a_n + (1 - 1/Z_n)\nu$, and dividing out Z_n. For the local propagator [Eq. (5)], $G^{d,n}_{\mathrm{loc},\nu} = Z_n G^{f,n}_{\mathrm{loc},\nu}$, this yields ($m \neq n$)

$$G^{f,n}_{\mathrm{loc},\nu} = \sum_{\boldsymbol{k}} \left[\nu - \epsilon^{f,n}_{\boldsymbol{k}} - \frac{(\epsilon^{f,\mathrm{io}}_{\boldsymbol{k}})^2}{\nu - \epsilon^{f,m}_{\boldsymbol{k}}} \right]^{-1},$$

$$\epsilon^{f,n}_{\boldsymbol{k}} = Z_n(\epsilon^{d,n}_{\boldsymbol{k}} + a_n), \quad (\epsilon^{f,\mathrm{io}}_{\boldsymbol{k}})^2 = Z_{\mathrm{lt}} Z_{\mathrm{hv}} (\epsilon^{d,\mathrm{io}}_{\boldsymbol{k}})^2.$$

Due to the factor $Z_{\mathrm{lt}} Z_{\mathrm{hv}}$, the interorbital hopping has no effect here if $Z_{\mathrm{hv}} = 0$. This agrees with our previous point that a dominant $|\Sigma^{\mathrm{hv}}_\nu|$ makes $G^{d,n}_{\mathrm{loc},\nu}$ independent of $\epsilon^{d,\mathrm{io}}_{\boldsymbol{k}}$. More insight is

obtained from the impurity propagator, $g^{d,n}_\nu = Z_n g^{f,n}_\nu$, with

$$g^{f,n}_\nu = \frac{1}{\nu - \epsilon^n_f - \Delta^{f,n}_\nu}, \quad \epsilon^n_f = Z_n(\epsilon^n_d + a_n), \quad \Delta^{f,n}_\nu = Z_n \Delta^{d,n}_\nu.$$

One finds that the f-fermion self-consistency condition ($G^{f,n}_{\mathrm{loc},\nu} = g^{f,n}_\nu$) leads to the same result for the d-fermion hybridization as in Eq. (7), now in the form $\Delta^{d,\mathrm{hv}}_\nu = \sum_{\boldsymbol{k}} (\epsilon^{d,\mathrm{io}}_{\boldsymbol{k}})^2 Z_{\mathrm{lt}} G^{f,\mathrm{lt}}_{\boldsymbol{k}\nu}$. This is still finite if the light orbital is metallic (here $Z_{\mathrm{lt}} > 0$). However, the crucial difference is that the impurity model for the slave spins is not characterized by $\boldsymbol{\Delta}^d_\nu$ but by $\boldsymbol{\Delta}^f_\nu$. Here, each component is tied to the quasiparticle weight, $\Delta^{f,n}_\nu = Z_n \Delta^{d,n}_\nu$. Hence, if $Z_{\mathrm{hv}} = 0$, the slave-spin impurity solver has no chance of seeing $\Delta^{d,\mathrm{hv}}_{\nu=0} \neq 0$ and, thereby, no chance of generating $Z_{\mathrm{hv}} > 0$ and leaving the OSMP. In other words, the inseparable connection of Z_n and $\Delta^{d,n}_\nu$ in slave-spin studies leads to additional stationary points of the free energy, not present in DMFT.

Conclusion—Using single-site DMFT, we showed that interorbital hopping t_{io} is a relevant perturbation to the OSMP and destabilizes it at $T = 0$ in favor of a Fermi-liquid ground state. The reason is that the low-energy hybridization in a given orbital has a finite contribution which stems from hopping to another orbital and back. Crucially, this term depends only on the availability of states in the intermediate orbital and not on the effective mass of the electron hopping. While an arbitrarily large imbalance in effective masses can still exist, within single-site DMFT, there is generically no OSMP with $t_{\mathrm{io}} > 0$ at $T = 0$ and more generally below the coherence scale. Its finite-temperature properties may thus be viewed as a coherence–incoherence crossover, where selected orbitals are localized for $T > T_{\mathrm{coh}}$ but itinerant for $T < T_{\mathrm{coh}}$. This crossover can either be tuned by increasing T in a given system [4] or by decreasing T_{coh} at fixed (nonzero) T (as in [7]).

Our analytic arguments are supported by numerical results using NRG as a DMFT impurity solver, capable of accessing real frequencies and arbitrarily low temperatures. This allowed us to demonstrate that T_{coh}, below which the Fermi-liquid properties are found, is very sensitive to system parameters and can be extremely small, even for moderate values of $t_{\mathrm{io}}/t_{\mathrm{lt}}$. We showed that many properties of the $t_{\mathrm{io}} \neq 0$ state for energies above T_{coh} are almost indistinguishable from the $t_{\mathrm{io}} = 0$ OSMP that reaches down to $T = 0$. Future theoretical work should aim to go beyond single-site DMFT to address the influence of nonlocal, interorbital self-energy components in renormalizing t_{io} [61]. Experimentally, our results can be tested by measuring the normal-state Fermi-surface volume at very low T and by analyzing the scaling behavior in the OSMP at $T > 0$.

the Feodor Lynen Fellowship.

———————

[1] M. Imada, A. Fujimori, and Y. Tokura, Rev. Mod. Phys. **70**, 1039 (1998).

[2] P. A. Lee, N. Nagaosa, and X.-G. Wen, Rev. Mod. Phys. **78**, 17 (2006).

[3] Q. Si, R. Yu, and E. Abrahams, Nat. Rev. Mater. **1**, (2016).

[4] M. Yi, Z.-K. Liu, Y. Zhang, R. Yu, J.-X. Zhu, J. Lee, R. Moore, F. Schmitt, W. Li, S. Riggs, J.-H. Chu, B. Lv, J. Hu, M. Hashimoto, S.-K. Mo, Z. Hussain, Z. Mao, C. Chu, I. Fisher, Q. Si, Z.-X. Shen, and D. Lu, Nat. Commun. **6**, (2015).

[5] Z. K. Liu, M. Yi, Y. Zhang, J. Hu, R. Yu, J.-X. Zhu, R.-H. He, Y. L. Chen, M. Hashimoto, R. G. Moore, S.-K. Mo, Z. Hussain, Q. Si, Z. Q. Mao, D. H. Lu, and Z.-X. Shen, Phys. Rev. B **92**, 235138 (2015).

[6] T. Otsuka, S. Hagisawa, Y. Koshika, S. Adachi, T. Usui, N. Sasaki, S. Sasaki, S. Yamaguchi, Y. Nakanishi, M. Yoshizawa, S. Kimura, and T. Watanabe, Phys. Rev. B **99**, 184505 (2019).

[7] J. Huang, R. Yu, Z. Xu, J.-X. Zhu, Q. Jiang, M. Wang, H. Wu, T. Chen, J. D. Denlinger, S.-K. Mo, M. Hashimoto, G. Gu, P. Dai, J.-H. Chu, D. Lu, Q. Si, R. J. Birgeneau, and M. Yi, arXiv:2010.13913.

[8] V. Anisimov, I. Nekrasov, D. Kondakov, T. Rice, and M. Sigrist, Eur. Phys. J. B **25**, 191 (2002).

[9] M. Neupane, P. Richard, Z.-H. Pan, Y.-M. Xu, R. Jin, D. Mandrus, X. Dai, Z. Fang, Z. Wang, and H. Ding, Phys. Rev. Lett. **103**, 097001 (2009).

[10] M. Vojta, J. Low Temp. Phys. **161**, 203 (2010).

[11] A. Georges, L. de' Medici, and J. Mravlje, Annu. Rev. Condens. Matter Phys. **4**, 137 (2013).

[12] F. Hardy, A. E. Böhmer, D. Aoki, P. Burger, T. Wolf, P. Schweiss, R. Heid, P. Adelmann, Y. X. Yao, G. Kotliar, J. Schmalian, and C. Meingast, Phys. Rev. Lett. **111**, 027002 (2013).

[13] Y. J. Pu, Z. C. Huang, H. C. Xu, D. F. Xu, Q. Song, C. H. P. Wen, R. Peng, and D. L. Feng, Phys. Rev. B **94**, 115146 (2016).

[14] H. Miao, Z. P. Yin, S. F. Wu, J. M. Li, J. Ma, B.-Q. Lv, X. P. Wang, T. Qian, P. Richard, L.-Y. Xing, X.-C. Wang, C. Q. Jin, K. Haule, G. Kotliar, and H. Ding, Phys. Rev. B **94**, 201109 (2016).

[15] N. Lanatà, Y. Yao, X. Deng, V. Dobrosavljević, and G. Kotliar, Phys. Rev. Lett. **118**, 126401 (2017).

[16] C.-W. Chen, W. Wang, V. Loganathan, S. V. Carr, L. W. Harriger, C. Georgen, A. H. Nevidomskyy, P. Dai, C.-L. Huang, and E. Morosan, Phys. Rev. B **99**, 144423 (2019).

[17] I. Giannakis, J. Leshen, M. Kavai, S. Ran, C.-J. Kang, S. R. Saha, Y. Zhao, Z. Xu, J. W. Lynn, L. Miao, L. A. Wray, G. Kotliar, N. P. Butch, and P. Aynajian, Sci. Adv. **5**, (2019).

[18] G. L. Pascut and K. Haule, arXiv:2005.12179.

[19] M. Kim, H.-S. Kim, K. Haule, and D. Vanderbilt, arXiv:2106.06204.

[20] A. Georges, G. Kotliar, W. Krauth, and M. J. Rozenberg, Rev. Mod. Phys. **68**, 13 (1996).

[21] G. Kotliar, S. Y. Savrasov, K. Haule, V. S. Oudovenko, O. Parcollet, and C. A. Marianetti, Rev. Mod. Phys. **78**, 865 (2006).

[22] L. de'Medici, A. Georges, and S. Biermann, Phys. Rev. B **72**, 205124 (2005).

[23] S. R. Hassan and L. de' Medici, Phys. Rev. B **81**, 035106 (2010).

[24] R. Yu and Q. Si, Phys. Rev. B **86**, 085104 (2012).

[25] P. Werner, E. Gull, and A. J. Millis, Phys. Rev. B **79**, 115119 (2009).

[26] L. de' Medici, S. R. Hassan, M. Capone, and X. Dai, Phys. Rev. Lett. **102**, 126401 (2009).

[27] T. Kita, T. Ohashi, and N. Kawakami, Phys. Rev. B **84**, 195130 (2011).

[28] L. Huang, L. Du, and X. Dai, Phys. Rev. B **86**, 035150 (2012).

[29] Y. Wang, L. Huang, L. Du, and X. Dai, Chin. Phys. B **25**, 037103 (2016).

[30] F. B. Kugler, S.-S. B. Lee, A. Weichselbaum, G. Kotliar, and J. von Delft, Phys. Rev. B **100**, 115159 (2019).

[31] See Refs. [22, 32–34] for how local interorbital hybridization affects the OSMP.

[32] A. Koga, N. Kawakami, T. M. Rice, and M. Sigrist, Phys. Rev. B **72**, 045128 (2005).

[33] L. de' Medici, A. Georges, G. Kotliar, and S. Biermann, Phys. Rev. Lett. **95**, 066402 (2005).

[34] Y. Komijani and G. Kotliar, Phys. Rev. B **96**, 125111 (2017).

[35] J. C. Slater and G. F. Koster, Phys. Rev. **94**, 1498 (1954).

[36] See, e.g., Table A.4 in Ref. [37] for iron pnictides and Tables S1 and S2 in the Supplemental Material of Ref. [38] for FeSe.

[37] K. Haule and G. Kotliar, New J. Phys. **11**, 025021 (2009).

[38] R. Yu, J.-X. Zhu, and Q. Si, Phys. Rev. Lett. **121**, 227003 (2018).

[39] R. Yu and Q. Si, Phys. Rev. Lett. **110**, 146402 (2013); Phys. Rev. B **96**, 125110 (2017).

[40] Z. P. Yin, K. Haule, and G. Kotliar, Phys. Rev. B **86**, 195141 (2012).

[41] LDA+DMFT had previously proven successful for iron pnictides and chalcogenides [42], and nonlocal correlations beyond single-site DMFT were later shown to be weak [43].

[42] Z. P. Yin, K. Haule, and G. Kotliar, Nat. Mater. **10**, 932 (2011).

[43] P. Sémon, K. Haule, and G. Kotliar, Phys. Rev. B **95**, 195115 (2017).

[44] Refs. [45, 46] argue for a stable OSMP including interorbital hopping using DMFT and a Lanczos impurity solver. They consider a two-orbital model with an identical real-space dependence of all hoppings and use a canonical transformation that kinetically decouples the orbitals. This is, however, not the generic situation, and such a decoupling scheme is impossible once the intra- and interorbital hoppings have different momentum dependencies.

[45] Y. Song and L.-J. Zou, Phys. Rev. B **72**, 085114 (2005); Eur. Phys. J. B **72**, 59 (2009).

[46] Y. Ni, J. Sun, Y.-M. Quan, and Y. Song, arXiv:2112.04664.

[47] R. Bulla, T. A. Costi, and T. Pruschke, Rev. Mod. Phys. **80**, 395 (2008).

[48] A. I. Poteryaev, M. Ferrero, A. Georges, and O. Parcollet, Phys. Rev. B **78**, 045115 (2008).

[49] M. Greger, M. Sekania, and M. Kollar, arXiv:1312.0100.

[50] A. C. Hewson, *The Kondo Problem to Heavy Fermions*, Cambridge Studies in Magnetism (Cambridge University Press, Cambridge, 1993).

[51] L. De Leo, *Non-Fermi liquid behavior in multi-orbital Anderson impurity models and possible relevance for strongly correlated lattice models*, Ph.D. thesis, SISSA (2004).

[52] C. Aron and G. Kotliar, Phys. Rev. B **91**, 041110 (2015).

[53] E. Walter, K. M. Stadler, S.-S. B. Lee, Y. Wang, G. Kotliar, A. Weichselbaum, and J. von Delft, Phys. Rev. X **10**, 031052 (2020).

[54] See the Supplemental Material at [url] for computational details, the bare density of states, numerical results away from half filling, analytic arguments for an arbitrary number of orbitals, and a discussion of the free-energy functional, which contains Refs. [65–76] listed below.

[55] Here, we use $T_{\mathrm{K}} = 0.4107\,(U\Gamma/2)^{1/2}\exp\!\left(-\frac{\pi U}{8\Gamma} + \frac{\pi\Gamma}{2U}\right)$, where $\Gamma = \pi\mathcal{A}_{\Delta,\nu=0}$; see Eq. (6.109) ff. in Ref. [50].

[56] Besides the local Hamiltonian, the shape of the DMFT hybridiza-

tion affects the Kondo temperature [57], too. Here, the only important aspect is that the exponential factor $\exp[-1/(\rho_0 J)]$ with $J \sim t^2/U$ remains the same.

[57] K. Held, R. Peters, and A. Toschi, Phys. Rev. Lett. **110**, 246402 (2013).

[58] Next to Hubbard bands, the insulating spectral function of the OSMP also features interband doublon-holon excitations (DHEs) [30, 59]. Using the techniques of Appendix B in Ref. [30] here, the Hubbard bands occur at energies $\pm(U + J)/2 = \pm 1.4$ and the DHEs at $\pm 3J = \pm 1.2$, so that the DHEs are not discernible.

[59] Y. Núñez Fernández, G. Kotliar, and K. Hallberg, Phys. Rev. B **97**, 121113 (2018).

[60] E. Müller-Hartmann, Z. Phys. B **76**, 211 (1989).

[61] L. De Leo, M. Civelli, and G. Kotliar, Phys. Rev. Lett. **101**, 256404 (2008).

[62] A. Weichselbaum, Ann. Phys. **327**, 2972 (2012); Phys. Rev. B **86**, 245124 (2012); Phys. Rev. Research **2**, 023385 (2020).

[63] S.-S. B. Lee and A. Weichselbaum, Phys. Rev. B **94**, 235127 (2016).

[64] S.-S. B. Lee, J. von Delft, and A. Weichselbaum, Phys. Rev. Lett. **119**, 236402 (2017).

[65] A. Weichselbaum and J. von Delft, Phys. Rev. Lett. **99**, 076402 (2007).

[66] F. B. Kugler, M. Zingl, H. U. R. Strand, S.-S. B. Lee, J. von Delft, and A. Georges, Phys. Rev. Lett. **124**, 016401 (2020).

[67] A. K. Mitchell, M. R. Galpin, S. Wilson-Fletcher, D. E. Logan, and R. Bulla, Phys. Rev. B **89**, 121105 (2014).

[68] K. M. Stadler, A. K. Mitchell, J. von Delft, and A. Weichselbaum, Phys. Rev. B **93**, 235101 (2016).

[69] F. B. Kugler, arXiv:2202.04063.

[70] R. Bulla, A. C. Hewson, and T. Pruschke, J. Phys.: Condens. Matter **10**, 8365 (1998).

[71] J. Kaufmann, P. Gunacker, A. Kowalski, G. Sangiovanni, and K. Held, Phys. Rev. B **100**, 075119 (2019).

[72] R. Žitko and T. Pruschke, Phys. Rev. B **79**, 085106 (2009).

[73] G. Kotliar, Eur. Phys. J. B **11**, 27 (1999).

[74] G. Kotliar, E. Lange, and M. J. Rozenberg, Phys. Rev. Lett. **84**, 5180 (2000).

[75] N. Blümer, *Mott–Hubbard metal-insulator transition and optical conductivity in high dimensions*, Ph.D. thesis, University of Augsburg (2002).

[76] E. G. C. P. van Loon, F. Krien, and A. A. Katanin, Phys. Rev. Lett. **125**, 136402 (2020).